ACS Catalysis

Research Article

pubs.acs.org/acscatalysis

Rational Design of a (S)-Selective-Transaminase for Asymmetric Synthesis of (1S)-1-(1,1′-biphenyl-2-yl)ethanamine

Daniel F. A. R. Dourado,[†,‡,▽] Stefan Pohle,[‡,▽] Alexandra T. P. Carvalho,[†,‡,▽] Dharmendra S. Dheeman,[‡] Jill M. Caswell,[‡] Timofey Skvortsov,[‡,§] Iain Miskelly,[‡] Rodney T. Brown,[‡] Derek J. Quinn,[‡] Christopher C. R. Allen,[§] Leonid Kulakov,[§] Meilan Huang,[*,†] and Thomas S. Moody[‡]

[†]School of Chemistry and Chemical Engineering, Queen's University Belfast, David Keir Building, Stranmillis Road, Belfast BT9 5AG, Northern Ireland, United Kingdom

[‡]Department of Biocatalysis and Isotope Chemistry, Almac Sciences, 20 Seagoe Industrial Estate, Craigavon BT63 5QD, Northern Ireland, United Kingdom

[§]School of Biological Sciences, Queen's University Belfast, Medical Biology Centre, 97 Lisburn Road, Belfast BT9 7BL, Northern Ireland, United Kingdom

Supporting Information

ABSTRACT: Amine transaminases offer an environmentally sustainable synthesis route for the production of pure chiral amines. However, their catalytic efficiency toward bulky ketone substrates is greatly limited by steric hindrance and therefore presents a great challenge for industrial synthetic applications. We hereby report an example of rational transaminase enzyme design to help alleviate these challenges. Starting from the *Vibrio fluvialis* amine transaminase that has no detectable catalytic activity toward the bulky aromatic ketone 2-acetylbiphenyl, we employed a rational design strategy combining *in silico* and *in vitro* studies to engineer the transaminase enzyme with a minimal number of mutations, achieving an high catalytic activity and high enantioselectivity. We found that, by introducing two mutations W57G/R415A, detectable enzyme activity was achieved. The rationally designed variant, W57F/R88H/V153S/K163F/I259M/R415A/V422A, showed an improvement in reaction rate by more than 1716-fold toward the bulky ketone under study, producing the corresponding enantiomeric pure (S)-amine (enantiomeric excess (ee) value of >99%).

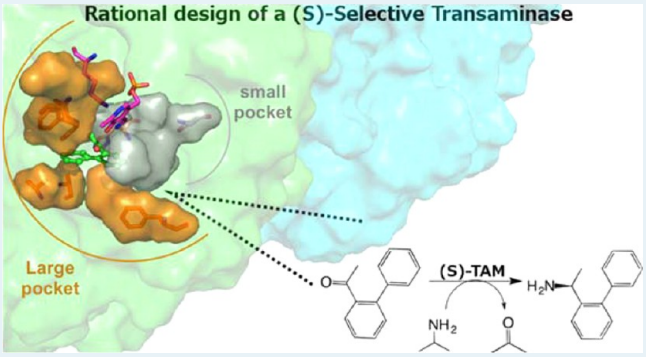

KEYWORDS: *biocatalysis, rational enzyme design, transaminases, molecular dynamics simulations, enzyme kinetics*

INTRODUCTION

There is high demand in the pharmaceutical and agrochemical industry for efficient synthesis of enantiomerically pure chiral amines, which are important building blocks for the preparation of pharmaceuticals and agrochemicals. As of 2006, 90% of the FDA approved drugs were chiral compounds.[1] Amine transaminases (TAms) offer a green synthesis route for the production of pure chiral amines.[2] TAms catalyze (in many instances with great stereoselectivity) the transfer of an amino group from a primary amine compound to a ketone compound and vice versa, using pyridoxal phosphate (PLP) as a cofactor. The generally accepted catalytic mechanism of TAms consists of two half reactions in a ping-pong bi−bi mechanism (Figure 1a).[3] In the first half reaction, an internal aldimine that is formed between a PLP bound to the enzyme (E:PLP) and a catalytic lysine reacts with the amino donor, yielding an external aldimine. A neutral lysine residue is released which then catalyzes internal hydrogen rearrangement via a planar quinonoid intermediate, yielding a ketimine. In the second half reaction, the ketimine is hydrolyzed, releasing the product ketone and yielding a pyridoxamine 5′-phosphate (PMP) bound to the enzyme (E:PMP). A ketimine complex then is formed between the E:PMP and the substrate ketone, which finally regenerates the E:PLP via a second planar quinonoid intermediate and external aldimine, yielding the secondary chiral amine product.

The catalytic site of these enzymes can accommodate ketones as well as amines and can be divided into large and small binding pockets (see Figure S1 in the Supporting Information).[4] The large binding pocket has a dual recognition capacity accommodating not only the bulky substituents of amines and ketones but also the carboxyl group of amino acids, pyruvate, etc.[4a] The small binding pocket adjacent to PLP

Received: August 19, 2016
Revised: September 26, 2016
Published: October 4, 2016

DOI: 10.1021/acscatal.6b02380
ACS Catal. 2016, 6, 7749−7759

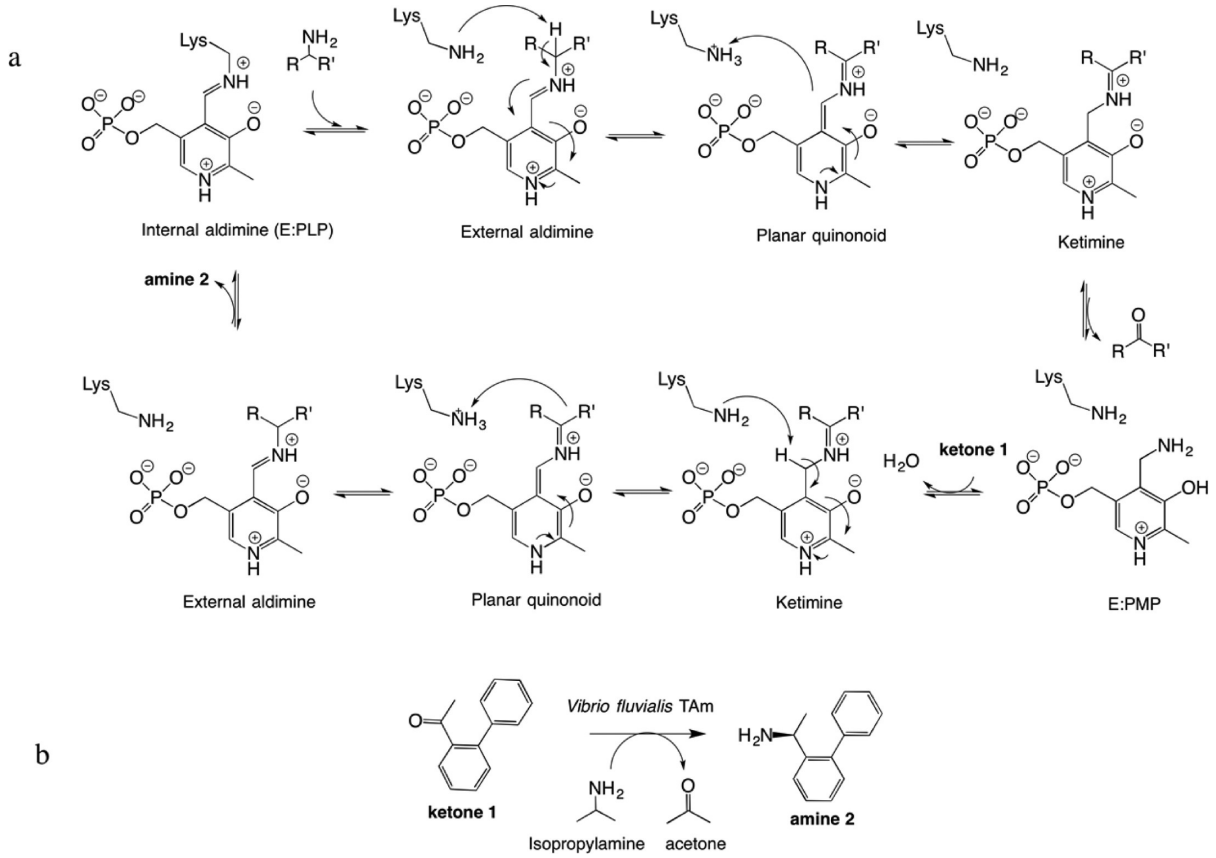

Figure 1. (a) General mechanism of the amine transaminase (TAm)-catalyzed transamination reaction where a ketone is converted to the corresponding amine. The upper panel shows the first half reaction and the lower panel shows the second half reaction. The intermediates investigated in this study were the E:PMP:substrate complex, the enzyme:planar quinonoid and the succeeding enzyme:external aldimine. (b). Asymmetric synthesis of (1S)-1-(1,1′-biphenyl-2-yl)ethanamine (amine **2**). The transamination reaction under study is between the substrate 2-acetylbiphenyl (ketone **1**) and the amine donor isopropylamine and catalyzed by *V. fluvialis* TAm.

accommodates small substituents and has a tendency to repel the carbonyl group of substrates.[4a]

The intrinsic promiscuous nature of these enzymes notwithstanding, their catalytic efficiency toward large ketone substrates is greatly limited by the steric hindrance.[4b] Therefore, it is necessary to expand the scope of these enzymes to accommodate bulkier substrates.

Some significant advances in the engineering of TAms have been achieved recently. One of the most relevant studies was the engineering of the (R)-selective-TAm from *Arthrobacter sp.* to produce sitagliptin starting from prositagliptin ketone.[5] The initial *modeling*-aided site-saturated mutagenesis protocol allowed the design of a mutated enzyme that provides a modest 0.7% conversion of prositagliptin ketone. Starting from this mutant, an impressive improvement in catalysis was achieved by numerous rounds of direct evolution that culminated in an enzyme with 89% conversion. However, 27 amino acids had to be mutated in this process.

The (S)-selective-TAms were also engineered to catalyze ketones larger than the native amine-acceptor pyruvate (Figure S2 in the Supporting Information).[6] Midelfort et al. obtained a rationally engineered *Vibrio fluvialis* TAm_F19W/W57F/F85A/R88K/V153A/K163F/I259V/R415F and improved the catalytic conversion of (R)-ethyl 5-methyl 3-oxooctanoate by 60-fold following an *in silico* and saturation mutagenesis protocol;[6a] Park et al. improved the amination of 2-oxo-octanoate by 4-fold with a *Paracoccus denitrificans* mutant TAm_V153A by following an alanine-scanning mutagenesis protocol that involved mutating six active site residues in the small binding pocket (L56, V153, F19, B:F85, L56, Y150, and L417).[6b] Han et al. studied in detail the transformation of some non-native ketones catalyzed by TAm from *Ochrobactrum anthropi* following an alanine-scanning mutagenesis protocol where the small-pocket-forming residues Y20, L57, W58, V154, F86, Y151, and B:T324 were mutated.[6c,d] They improved the reaction rate of this TAm toward butyrophenone by 110-fold with mutant L57A[6d] and improved the k_{cat}/K_M toward acetophenone by 340-fold with mutant W58L.[6c] Moreover, advances have also been made for the conversion of relevant amines into ketones and aldehydes by mutating *V. fluvialis* TAm. Nobili et al. increased the conversion of (S)-1-phenylbutylamine to the corresponding ketone by 30-fold with TAm_F85L/V153A,[6e] Genz et al. observed an ∼3-fold improvement in the conversion of the same amine to pentanal by mutating W57 and R415,[6f] Cho et al. observed an ∼41-fold improvement in the conversion of 4-phenylbutylamine by mutating W57.[6g]

However, when compared with the aforementioned (R)-selective TAm case,[5] the improvement in the catalytic efficiency of (S)-selective TAms is moderate and the ketone substrates are not significantly bulkier than the native substrates. Further efforts are necessary to obtain an efficient (S)-selective-TAm that can convert bulky ketone substrates, producing pure chiral amine compounds.

DOI: 10.1021/acscatal.6b02380
ACS Catal. 2016, 6, 7749−7759

In this study, we rationally engineered the (S)-selective TAm from *V. fluvialis* to catalyze 2-acetylbiphenyl (ketone **1**) to the corresponding amine (amine **2**), using isopropylamine, which has been suggested to be an ideal amino donor for asymmetric amination of ketones (Figure 1b). The wild type (WT) enzyme showed no detectable catalysis toward the bulky ketone **1** while the best variant with only seven mutations converted 42% of 1 g/L of the substrate, yielding the corresponding (S)-amine product with an enantiomeric excess (ee) value of >99% (see Table 1). This corresponds to an improvement of more than 1716-fold in the reaction rate (see Table 1).

The rational design in this study is based on an iterative strategy that combines state-of-the-art *in silico* procedures with *in vitro* methodologies to engineer TAms as new biocatalysts. The high conversion efficiency associated with the engineered enzyme adds an excellent example in the existing scarce successes in expanding the substrate scope of the enzymes to obtain pure chiral amine products. This strategy substantially decreases the screening effort requested by traditional directed evolution methods based on error-prone polymerase chain reaction, DNA shuffling and saturation mutagenesis, and provides a new approach in reshaping the binding pocket of the enzymes to catalyze industrially impeded reactions.

METHODS

The designed *V. fluvialis* TAm variants resulted from an iterative rational strategy that involves exhaustive structural analysis, molecular docking, molecular dynamics (MD) simulations, quantum mechanics (QM) calculations, *in silico* protein structural stability study, coevolution network analysis, and *in vitro* screening. In total, 113 mutants were rationally designed and assessed *in vitro*.

Computational Methods. The substrate ketone **1** (Figure 1b, as well as Figure S2a) was docked into the WT *V. fluvialis* TAm (PDB code: 4E3Q)[6a] and to the rationally designed mutants. The enzyme was modeled in the presence of the PMP co-factor intermediate (see Figure S7a in the Supporting Information). All systems were subsequently submitted to MD simulations (the root-mean-square deviation (RMSD) of the α-C atoms can be seen in Figure S11 in the Supporting Information). To assess the enantioselectivity of the selected *V. fluvialis* variants, we docked the planar quinonoid into them. For the best variant, we additionally analyzed the pro-(S) external aldimine intermediate. Both the planar quinonoid and the pro-(S) external aldimine structures of the best variant were submitted to MD simulations (RMSD of the α-C atoms can be seen in Figures S12 and S13 in the Supporting Information).

Parameterization of the Substrate. The geometries of the substrate ketone **1** and its corresponding planar quinonoid and pro-(S) external aldimine intermediates were initially optimized in Gaussian 09,[7] using the density functional theory (DFT) method with the exchange-correlation functional B3LYP and the 6-31g(d) basis set,[8] following a procedure employed in the previous literature.[9] The effect of solvent was approximately considered using the Polarizable Continuum Model (PCM),[10] as implemented in Gaussian 09, with the dielectric constant of water being set to 80. Atomic point charges were then calculated by fitting the HF/6-31g(d) generated electrostatic potential to atomic point charges using the RESP algorithm.[11] These point charges were subsequently used in the docking calculations and MD simulations.

Molecular Docking. Starting with the WT crystal structure, the models of the variants were built using the mutation tool and side chain rotamer search algorithm of the Swiss PDB viewer software.[12] Molecular docking was performed using the AutoDock 4.2 suite with the Lamarckian genetic algorithm (LGA) and the standard free-energy scoring function.[13] A grid box was centered on the amino group of the PMP cofactor. The catalytic lysine was deprotonated. A total of 100 LGA runs were carried out for each ligand:protein complex. The population was 300, the maximum number of generations was 27 000, and the maximum number of energy evaluations was 2 500 000. For each system analyzed, the top-ranked structure corresponds to the lowest binding energy structure of the most populated cluster with the lowest mean binding energy.

Molecular Dynamics. Molecular dynamics (MD) simulations were performed for the WT enzyme and the variants using the Amber MD program (AMBER14)[14] with the parm99SB[15] and GAFF[16] force fields. The structures were placed within a truncated octahedral box (spacing distance of 10 Å) of TIP3P waters and counterions were added to neutralize the system. The systems were first subjected to two energy minimizations, using the steepest descent and conjugate gradient algorithms and were subsequently slowly heated to 300 K during 50 ps with small restraints of 10 kcal/mol/Å (to all atoms except waters and ions) in an NVT ensemble using Langevin dynamics. For each system under study, three 10 ns production simulations with random initial velocities were carried out at 300 K in the NPT ensemble using Langevin dynamics with a collision frequency of 1.0 ps^{-1}. Constant pressure periodic boundary conditions were imposed with an average pressure of 1 atm. Isotropic position scaling was used to maintain pressure with a relaxation time of 2 ps. The time step was set to 2 fs. SHAKE constraints were applied to all bonds involving hydrogen atoms.[17] The particle mesh Ewald (PME) method was used to calculate electrostatic interactions with a cutoff distance of 10 Å.[18]

Coevolution Network. The coevolution network of PLP-dependent aminotransferase superfamily—the Ornithin-trans-aminase-like family (~30 000 sequences)—was calculated using Comulator software.[19,20] Standard parameters were used.

Prediction of Binding Energy. We used the Zone Equilibration of Mutants (ZEMu) protocol to predict the change in binding free energy upon amino acid substitution ($\Delta\Delta G$),[21] as implemented in MMB.[22] In this protocol, first, a flexibility zone is defined, which includes the residue to be mutated plus two residues on each side. The flexibility zone is treated in torsion space while the rest of protein is rigid. A *physics zone* then is established. This includes all residues within 12 Å of the *flexibility zone*, inside of which PARM99 electrostatic and van der Waals forces are active. After equilibration of the *flexibility zone*, the energy is evaluated with the KB potential FoldX.[23] The calculation is performed for both the WT free energy (ΔG_{wt}) and the mutant free energy (ΔG_{mut}). An estimate of the experimental change in binding free energy ($\Delta\Delta G_{exp}$) is obtained as follows:

$$\Delta\Delta G_{exp} = \Delta G_{mut} - \Delta G_{wt}$$

Experimental Methods. *Chemicals.* The starting material ketone **1** (Figure 1b, as well as Figure S2a) was purchased from Fluorochem (Hadfield, U.K.) and the product standard (1S)-1-(2-biphenylyl)ethanamine was purchased from AP Bioscience, LLC (Princeton, NJ, USA). 1-Acetophenone was purchased from Sigma−Aldrich (Dorset, U.K.) and racemic α-methylbenzylamine was obtained from Alfa Aesar (Heysham, U.K.). PLP was obtained from Alfa Aesar (Heysham, U.K.),

DOI: 10.1021/acscatal.6b02380
ACS Catal. 2016, 6, 7749−7759

isopropylamine hydrochloride from Tokyo Chemical Industry UK, Ltd. (Oxford, U.K.) and monobasic and dibasic potassium phosphate from Sigma−Aldrich (Dorset, U.K.). Components of bacterial cultures were purchased from Sigma−Aldrich (Dorset, U.K.), VWR Chemicals (Lutterworth, U.K.), kanamycin was purchased from ForMedium (Hunstanton, U.K.), and isopropylthiogalactosid (IPTG) was purchased from Carbosynth (Compton, U.K.).

Gene Synthesis and Cloning. The genes for the *V. fluvialis* TAm WT and mutant variants designed in this work were commercially synthesized by GenScript (Piscataway, NJ, USA). All TAm genes were cloned into the pET28a(+) vector using *Eco*RI and XhoI restriction sites and transformed into *E. coli* BL21(DE3) cells (Thermo Fisher Scientific).

Transaminase Screening. Transformed *E. coli* BL21(DE3) clones carrying TAm variant plasmids were transferred into the wells of 96-deep well plates containing 500 μL of LB medium (10 g/L NaCl, 10 g/L tryptone, 5 g/L yeast extract) supplemented with 50 μg/mL kanamycin. Plates were sealed with breathable heat seals and incubated at 37 °C and 1400 rpm in a plate incubator (Model MB100-4A, Hangzhou Allsheng Instruments Co., Ltd., China) overnight. For protein expression, 10 μL of preculture was transferred into 490 μL of fresh LB medium supplemented with 50 μg/mL kanamycin in new 96-deep well plates. The plates were sealed with breathable heat seals and incubated for 2−3 h, followed by the addition of IPTG to a final concentration of 1 mM. Plates were resealed with breathable seals and further incubated at 25 °C and 1400 rpm. Subsequently, the cells were pelleted by centrifugation at 4500 rpm (Model Rotina 420, Hettich, Beverly, MA), the supernatant was discarded, and the plate with the cell pellets was frozen at −20 °C.

For TAm activity screenings, plates were thawed and 180 μL of phosphate buffer (pH 8) containing 0.56 mM PLP and 0.56 M isopropylamine hydrochloride were added to the cell pellet of each well. Following the addition of 20 μL of 51 mM ketone **1**, plates were sealed with aluminum foil heat seals and incubated at 40 °C and 1500 rpm in a plate incubator for 18 h. Reactions were stopped by the addition of 800 μL of 62.5% acetonitrile, followed by resealing of the reaction plates and mixing at 1500 rpm in the plate incubator. Subsequently, reactions were centrifuged for 15 min at 4500 rpm (Model Rotina 420, Hettich, Beverly, MA) and supernatants were analyzed by high-performance liquid chromatography (HPLC).

Preparation of TAm Cell-Free Extract. One liter (1 L) of LB medium (10 g/L NaCl, 10 g/L tryptone, 5 g/L yeast extract) supplemented with 50 μg/mL kanamycin was inoculated with 10 mL of an overnight culture and incubated at 37 °C and 180 rpm (Forma Orbital Shaker Model 491, Thermo Scientific) until an optical density (OD) of 0.6 was reached. Subsequently, protein expression was induced by the addition of IPTG to a final concentration of 1 mM, followed by an overnight incubation at 25 °C. After incubation, cells were harvested by centrifugation at 4 °C and 6000 rpm (Sorvall RC 6 plus, Thermo Scientific), resuspended in 0.1 M potassium phosphate containing 0.25 mM PLP, and sonicated for 8 cycles of 10 s and cooled on ice. Following centrifugation at 6000 rpm (Sorvall RC 6 Plus, Thermo Scientific) and 4 °C, supernatants were freeze-dried and the obtained cell free extract powder stored at 4 °C.

Purification of WT TAm and Its Variants. For protein purification, wild-type TAm and the four variants described in Table 1 were expressed in *E. coli* BL21 (DE3). Cells bearing plasmid pET28a-*TAm* were cultured at 37 °C in 1 L of LB medium containing 50 μg/mL kanamycin to mid log phase (A600 nm ∼0.6). Before protein induction, with 1 mM IPTG, LB medium was allowed to cool to 25 °C and, after induction, further incubated at 25 °C and 200 rpm for 18 h. The induced culture was centrifuged at 5000 rpm at 4 °C for 10 min, suspended in 20 mL of buffer A consisting of 50 mM sodium phosphate buffer, pH 7.4, containing 0.3 M NaCl and 20 mM imidazole to which protease inhibitor cocktail (cOmplete Mini, EDTA-free, Roche Diagnostics GmbH, Germany) was added to a final 1× concentration. The cells were lysed on ice using sonication (Soniprep 150, MSE, Ltd., U.K.) at an amplitude of 16 μm for 9 cycles (10 s pulse and 10 s pause) for 3 min and centrifuged at 12 000 rpm for 30 min. The supernatant was filtered through a 0.22 μm syringe filter unit (Millex-GP, Merck Millipore, Ltd., Ireland) and loaded onto a 2 mL HisPur Cobalt Resin (Thermo Scientific, IL USA) column, pre-equilibrated with 5 column volumes of buffer A. The column was washed (1.7 mL/min) with 50 column volumes of buffer A before TAm was eluted (0.7 mL/min) with 2 column volumes of buffer A containing 0.25 M imidazole and protease inhibitor cocktail. Imidazole was removed, and the protein was concentrated to 0.5 mL by centrifugation, washing three times with 1 mL of buffer A containing no imidazole, with a centrifugal filter with 3000 MWCO membrane (Amicon Ultracel 3K, Millipore, Ltd., Ireland). Glycerol was added to 10% (v/v), and the purified protein was distributed in 50 μL aliquots, flash-frozen in liquid nitrogen and stored at −80 °C until use. Protein concentrations were determined by micro BCA protein assay kit (Thermo Scientific, Rockford, IL, USA) using BSA as a standard.

Transaminase Assay. Unless otherwise specified, TAm enzyme reactions were prepared in 96-deep well plates by mixing 100 μL of 20 mg/mL cell-free TAm extract in phosphate buffer (pH 8) with 80 μL of phosphate buffer (pH 8) containing 2.5 mM PLP and 2.5 M isopropylamine hydrochloride, followed by the addition of 20 μL of 51 mM ketone **1**. Plates were sealed with aluminum foil heat seals and incubated at 40 °C and 1500 rpm in a plate incubator (Model MB100-4A, Hangzhou Allsheng Instruments Co., Ltd., China) for 18 h.

Reactions were stopped by addition of 800 μL 62.5% acetonitrile, followed by resealing of the reaction plates and mixing at 1500 rpm in the plate incubator. Subsequently, reactions were centrifuged for 15 min at 4500 rpm (Model Rotina 420, Hettich, Beverly, MA) and supernatants were analyzed by HPLC.

Determination of Kinetic Parameters. Apparent kinetic parameters of the purified enzymes were obtained under pseudo-one-substrate conditions. Initial rate measurements were performed with varying concentrations of substrates (0.2−200 mM for acetophenone, 0.025−25 mM for ketone **1**), while keeping the concentration of amine donor (IPA) constant at 1 M. HPLC analysis was used to monitor the progress of the reactions. The kinetic parameters (K_M and k_{cat}) were estimated by nonlinear regression of the initial reaction rates using GraphPad Prism 6 (GraphPad Software, Inc., USA).

HPLC Analysis. Ketone 1. Sample analysis was performed using an Agilent 1290 U-HPLC system equipped with a Kinetix C18 column (2.1 mm × 50 mm, 100A, 1.7 μm, Phenomenex, Macclesfield, U.K.) heated to 40 °C using 0.1% phosphoric acid as mobile phase A and MeCN (190 far-UV grade, Romil, Waterbeach, U.K.) supplemented with 0.1% phosphoric acid as mobile phase B. Sample volumes of 1−10 μL were injected and

DOI: 10.1021/acscatal.6b02380
ACS Catal. 2016, 6, 7749−7759

Table 1. Transamination of Ketone 1 by the *V. fluvialis* TAm and Engineered Variants

	WT	W57G/R415A	W57G/K163F/ R415A	W57G/I259M/ R415A	W57F/R88H/V153S/K163F/I259M/R415A/ V422A
ee (%) (*S*)-amine	ND[a]	>99	>99	>99	>99
conversion[b] (mean ± SD, %)	ND[a]	2.49 ± 0.11	5.63 ± 0.64	1.9 ± 0.13	42.14 ± 0.89
K_M[c] [mM]	NA	0.263	0.405	0.188	0.155
k_{cat}[c] [s^{-1}]	NA	7.88×10^{-4}	3.29×10^{-3}	1.19×10^{-3}	6.68×10^{-3}
k_{cat}/K_M [M^{-1} s^{-1}]	NA	3.00	8.13	6.30	43.0
fold increase in k_{cat}/K_M[d]	NA	1	3	2	14
reaction rate[e] [μM/h]	ND[a,f]	14.3	36.2	14.4	171.6
reaction rate fold increase		>143	>362	>144	>1716

[a]ND = not detectable. [b]Reaction conditions: 5 mM substrate, 1 M IPA, 0.01 mM of purified enzyme (see Figure S14 in the Supporting Information), 0.1 M potassium phosphate buffer (pH 8.0), 10% DMSO (v/v), 40 °C, 18 h. All reactions were performed in triplicates. [c]Kinetic parameters are the apparent rate constants calculated from the initial reaction rates at a fixed concentration of amine donor (1 M). [d]Fold change with W57G/R415A as reference. [e]Reaction rates are initial reaction rates. Reaction conditions: 5 mM substrate, 1 M IPA, 0.01 mM of purified enzyme, 0.1 M potassium phosphate buffer (pH 8.0), 10% DMSO (v/v), 40 °C. Reactions were performed in duplicates. [f]The reaction rate for WT was no more than 0.1 μM/h, considering the detection limit.

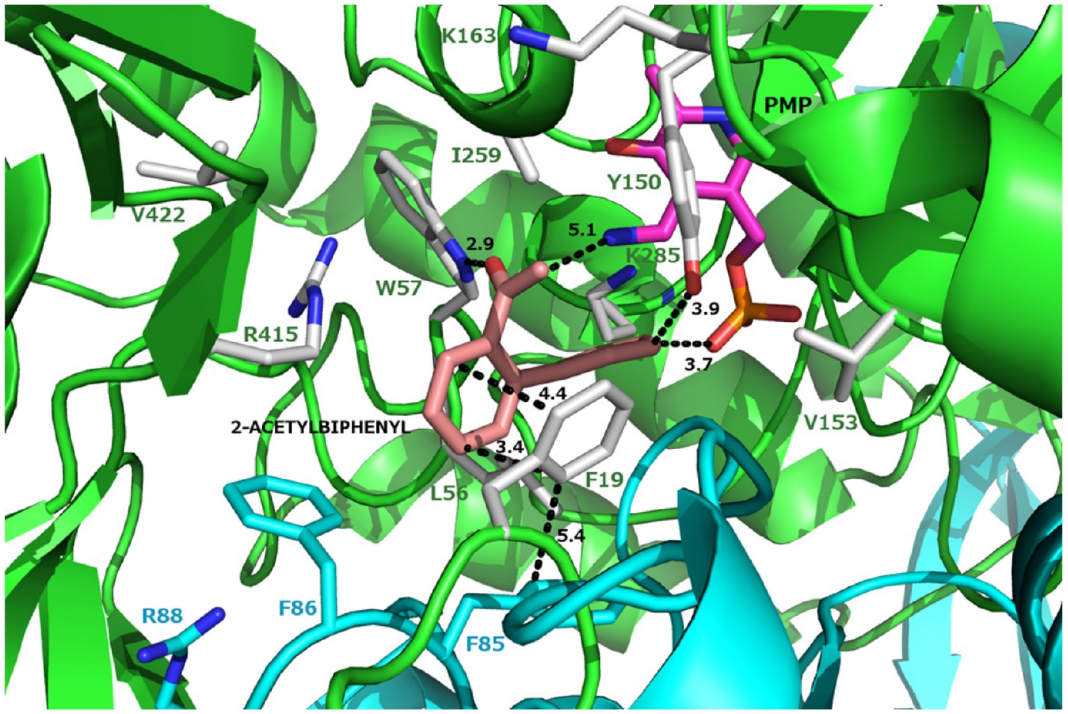

Figure 2. MD reference structure of ketone **1** docked to WT *V. fluvialis* TAm in the presence of PMP. The active center residues are represented by sticks with the carbons of Chain A (green ribbon) colored in gray and the carbons of Chain B (cyan ribbon) colored in cyan. Relevant distances are shown (in units of Å). The MD reference structure corresponds to the structure with the lowest RMSD (α-C atoms), relative to the average structure of the simulation. No significant changes were observed in the MD replicas.

analyzed in the following gradient run: 10% mobile phase B to 95% mobile phase B in 1.0 min, followed by 0.5 min at 95% mobile phase B and 0.5 min at 10% mobile phase B at a flow rate of 0.5 mL/min. Conversion of ketone **1** was observed at 210 nm.

For chiral analysis, the Agilent 1290 U-HPLC system was used with an Amylose 2 column (4.6 × 150 mm, 1.7 μm, Phenomenex, Macclesfield, U.K.) heated to 45 °C. Sample volumes of 10 μL were injected and analyzed in a 15 min isocratic run of 65% 0.1% ammonium hydroxide/35% MeCN at a flow rate of 1 mL/min. Formation of amine product enantiomers was observed at 210 nm.

Acetophenone. Sample analysis was performed using an Agilent 1290 U-HPLC system equipped with a Kinetex C18 column (3 × 100 mm, 100 Å, 2.6 μm, Phenomenex, Macclesfield, U.K.) heated to 40 °C using 0.1% phosphoric acid as mobile phase A and MeCN (190 far-UV grade, Romil, Waterbeach, U.K.) supplemented with 0.1% phosphoric acid as mobile phase B. Sample volumes of 1−10 μL were injected and analyzed in the following gradient run: 5% mobile phase B to 95% mobile phase B in 3.0 min, followed by 1 min at 95% mobile phase B and 1.2 min at 5% mobile phase B at a flow rate of 0.5 mL/min. A conversion of acetophenone was observed at 210 nm.

Racemic 1-(2-Biphenylyl)ethanamine Standard Synthesis. A mixture of 60 mg of ketone **1**, 116 mg of ammonium formate, and 60 mg of zinc in 0.7 mL of ethanol was heated to reflux under argon overnight. Additional amounts of zinc (3 equiv) and ammonium formate (6 equiv) were added and heated under continuous reflux overnight. The reaction mixture was

DOI: 10.1021/acscatal.6b02380
ACS Catal. 2016, 6, 7749−7759

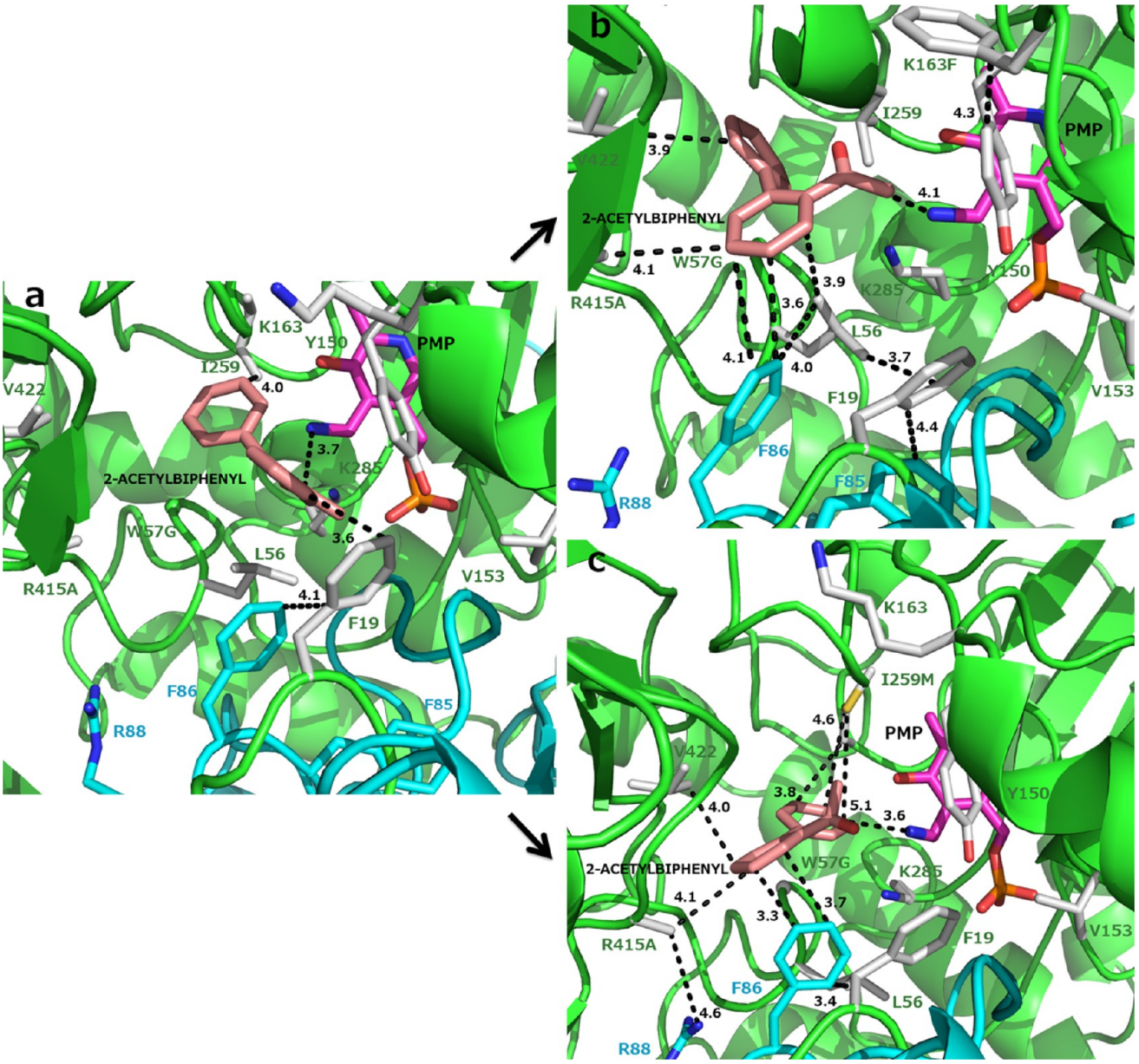

Figure 3. MD reference structures of ketone **1** docked to *V. fluvialis* TAm mutants in the presence of PMP: (a) TAm_W57G/R415A, (b) TAm_W57G/K163F/R415A, and (c) TAm_W57G/I259M/R415A. The active center residues are represented by sticks with the carbons of Chain A (green ribbon) colored in gray and the carbons of Chain B (cyan ribbon) colored in cyan. Relevant distances are shown (in units of Å). The MD reference structure corresponds to the structure with lowest RMSD (α-C atoms), relative to the average structure of the simulation. No significant changes were observed in the MD replicas.

filtered through Celite and washed with ethanol. The filtrate was concentrated on a rotary evaporator at 40 °C to leave a whitish oil, followed by the addition of 10 mL of 1 M HCl and washing with diethyl ether (2× 20 mL). The aqueous layer was basified to pH 10 with ammonium hydroxide and extracted with DCM (1× 10 mL, 2× 5 mL). The organic layer was washed with 10 mL of brine and dried over Na_2SO_4. Finally, it was concentrated on a rotary evaporator and 12 mg of clear oil was obtained.

Thermal Stability. The thermal stability of the WT and the variants described in Table 1 was measured. The reactions were carried out with 5 mM ketone **1**, 1 M IPA, 0.01 mM enzyme, 0.1 M potassium phosphate buffer (pH 8.0), 10% dimetyhl sulfoxide (DMSO) (v/v). Enzymes in phosphate buffer were preincubated in 96-well plates at 40, 50, and 60 °C for 18 h. Reactions with the preincubated enzyme were set up the next day, in parallel with control reactions. Reactions were carried out at the same temperature that was used for preincubation. After 4 h, the reactions were quenched with 62.5% acetonitrile and analyzed using HPLC. All reactions were performed in triplicate.

RESULTS AND DISCUSSION

So far, there has been limited success in the engineering of (S)-selective TAm enzymes to catalyze significantly large ketone substrates,[6a−d] when compared with the improvements obtained for a (R)-selective TAm enzyme.[5] Here, we have studied the conversion of ketone **1** by the homodimeric *V. fluvialis* TAm (see Figure 1b, as well as Figure S2a). It is worth noting that ketone **1** is larger than the substrates studied in the

DOI: 10.1021/acscatal.6b02380
ACS Catal. 2016, 6, 7749−7759

previous research (Figure S2).[6a−d] A substrate (R)-ethyl 5-methyl 3-oxooctanoate (Figure S2b) has a similar molecular weight; however, it is less bulky than ketone **1**. In addition, until completion of this present work, WT *V. fluvialis* TAm has shown no detectable catalysis toward ketone **1** (Table 1), while all other studies started with measurable activities with the respective WT TAms. The design of the initial *V. fluvialis* TAm variants resulted from an exhaustive structural analysis, molecular docking, and MD simulations. After initial simulations for the WT *V. fluvialis* TAm, we observed that the substrate ketone **1** is essentially held in place by a π-stacking interaction with the side chain of F19 and a strong hydrogen bond with the indole side chain of the residue W57 (Figure 2). However, this seems to be a noncatalytic pose, because the distance between the amino group of PMP and the ketone **1** carbonyl is large (5.1 Å) and the phenyl group of ketone **1** is turned to PMP. Thus, the PMP nucleophilic attack to the ketone **1** carbonyl carbon seems highly improbable, since the approximation of the substrate to PMP would involve considerable steric clash (Figure 2).

As can be seen from the MD simulation of the WT TAm (Figure 2), the bulky W57 is placed in the middle of the active center and it does not provide a space large enough to accommodate the bulky substrate in a catalytic pose. Therefore, it is imperative to mutate W57 to smaller nonpolar residue. In all our mutants, this residue was mutated to alanine, glycine, or phenylalanine, respectively (see Table S1 in the Supporting Information). Previous studies on ω-TAms indicated that the enzymes' specificity is highly dependent on the binding step rather than the subsequent catalytic step.[24] Thus, mutations introduced in the large binding pocket would not only open the pocket but also create strong intermolecular interactions with the substrate. Therefore, in addition to W57, we also focused our attention on other relevant binding pocket residues (K163, A228, E257, V258, I259, V422, R415) (see Figure S1 and Table S1). On the other hand, the small binding pocket residues are positioned in the vicinity of the interface of the subunits. Thus, it could negatively alter the intrinsic stability of the enzyme if this pocket is excavated to fit a bulky substrate. Therefore, we mutated only five residues of this pocket, namely, G55, L56, H83, B:R88, and V153 (Figure S1 and Table S1), in order to enhance the intermolecular interactions in the subunit interface and, therefore, the enzyme overall structural stability. Because of the nonpolar nature of the ketone substrate, it is imperative to decrease the overall charge of active center. Positions R88, K163, and R415 in *V. fluvialis* TAm were mutated in the synthesis of imagabalin.[6a] However, in the best variant reported, the residue at position 88 was still mutated to a positively charged lysine residue. In the present study, we decreased the overall active site charge by mutating the positively charged residues R88, K163, and R415. In addition, we also mutated residues that interact with PMP, L56, and B:R88 (see Table S1).

In total, 72 mutants were assessed experimentally in the first round of *in vitro* screening, from which several initially designed mutants were validated to have a detectable conversion of the substrate. Those involved positions 57, 88, 153, 163, 259, 415, 422 (Table S1), among which the most efficient double mutant is *V. fluvialis* TAm W57G/R415A (Table 1). Subsequently, we designed multiple variants based on the screening results, structural analysis, and the calculated evolution correlation network. The first-round screening results and structural analysis indicated that better activity could be achieved by combining *V. fluvialis* TAm W57G/R415A with mutations at positions 88, 163, 259. The evolution correlation network of the active center residues based on analysis of 30 000 homologous sequences disclosed obvious correlation between I259 and residues V153 and V422 (see Figure S3 in the Supporting Information). This was also taken into account in the design of the new multiple mutants.

The designed multiple mutants were examined *in silico* using molecular docking and MD simulations (the latter were based on the best docking results) and then assessed experimentally in a second round of *in vitro* screening (41 multiple mutants) (see Table S1).

Best Mutants Identified from Rational Design. The best *V. fluvialis* TAm mutant identified from the first-round *in vitro* screening was W57G/R415A (Figure 3a). Introduction of the W57G substitution enlarges the active center pocket and adds extra flexibility to the loop where this residue is located. As a result, the phenyl group of ketone **1** is now far from PMP. It occupies the space vacated by the loss of the tryptophan residue and establishes London dispersion forces with the side chain of I259. The R415A substitution further opens the active center pocket and decreases the positive charge (Figure 3a) of the pocket, contributing to an increase in the affinity for the hydrophobic substrate. The distance between the ketone **1** carbon and the PMP amino nitrogen decreases to 3.7 Å, which is a much more reasonable distance for the nucleophilic attack than that observed in the WT enzyme. This distance is also comparable with the reported distance of 2.65 Å for a PMP:acetophenone intermediate along the reaction path of the related *Chromobacterium violaceum* TAm, which was obtained from density functional theory calculations.[25] This double mutant provided an experimental conversion of 2.49% for ketone **1**, which corresponds to an improvement in the reaction rate by more than 143-fold (see Table 1).

Based on the promising catalytic activities exhibited in the first-round *in vitro* screening, new mutants of *V. fluvialis* TAm were designed and tested in a second-round *in vitro* screening (Table S1). Here, we describe, in detail, two of the best triple mutants, as well as the overall best multiple mutant identified from the second-round screening. One of those is the variant TAm_W57G/K163F/R415A. It should be noted that a phenylalanine at position 163 is rarely observed in the analyzed homologous sequences (Figure S4 in the Supporting Information). Only ∼0.4% of those sequences have a phenylalanine and the most common residues are the polar glutamine and asparagine residues, as well as the charged lysine (Figure S4). However, because of the nonpolar nature of ketone **1**, it was imperative to decrease the overall charge of the active center. To achieve this, a new variant was designed where the positively charged residues K163 and R415 were mutated into neutral residues. In this variant, the hydrophobicity of the active center is increased while the charged R415 and K163 residues were simultaneously mutated into nonpolar residues alanine and phenylalanine, respectively (Figure 3b). The substrate establishes a strong π-stacking interaction with Phe86 of Chain B and is also involved in London dispersion forces with the side chains of residues L56, A415, and V422. The distance between the ketone **1** carbon and the PMP amino nitrogen is 4.1 Å (Figure 3b). *In vitro* analysis demonstrated that this mutant reached 5.63% conversion of ketone **1**, which is an improvement in catalytic efficiency by 3-fold over the double mutant (Table 1).

DOI: 10.1021/acscatal.6b02380
ACS Catal. 2016, 6, 7749−7759

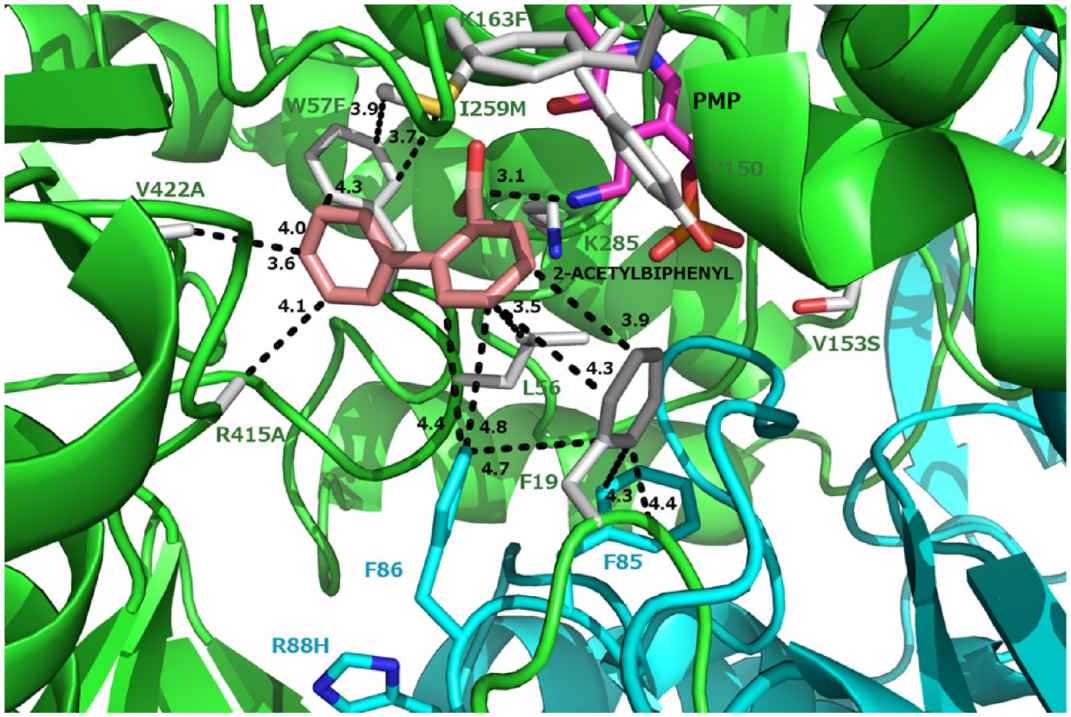

Figure 4. MD reference structure of ketone **1** docked to *V. fluvialis* TAm W57F/R88H/V153S/K163F/I259M/V422A/R415A in the presence of PMP. The active center residues are represented by sticks with the carbons of Chain A (green ribbon) colored in gray and the carbons of Chain B (cyan ribbon) colored in cyan. Relevant distances are shown (in units of Å). The MD reference structure corresponds to the structure with lowest RMSD (α-C atoms), relative to the average structure of the simulation. No significant changes were observed in the MD replicas.

The second triple mutant *V. fluvialis* TAm W57G/R415A/I259M was designed to introduce a S/π interaction between the sulfur atom of the methionine residue 259 and the aromatic phenyl group of ketone **1** (Figure 3c). S/π interactions between the methionine sulfur and aromatic rings are stronger than hydrophobic interactions and are known to have an important role in protein stabilization.[26] In addition, the methionine is less prone to oxidation while forming a stable S/π interaction. Therefore, it is beneficial to introduce such interactions in the rational design of enzymes.[27] Similar to the other triple mutant (Figure 3b), we also observed a strong π-stacking interaction between ketone **1** and the side chain of Phe86 from Chain B, as well as London dispersion forces between the substrate and the side chains of residues L56, A415, and V422 (Figure 3c). The distance between the carbonyl carbon atom of ketone **1** and the amino nitrogen atom of PMP is decreased to 3.6 Å. The catalytic efficiency improves by 2-fold over the double mutant (Table 1).

Based on the initial *in vitro* screening results, the coevolution network, and molecular modeling, we also designed multiple variants with 4−7 substitutions (Table S1). Among them, one variant (Figure 4) W57F/R88H/V153S/K163F/I259M/R415A/V422A exhibits significantly improved activity. The catalytic efficiency improves by 14-fold over the double mutant (Table 1). It converts up to 42.14% of ketone **1** at 1 g/L of substrate (Table 1) and corresponds to an improvement of the reaction rate by more than 1716-fold. This variant also shows an improvement in the reaction rates and kinetic parameters toward acetophenone, which is a standard TAM substrate (see Table S2 in the Supporting Information).

As previously mentioned, because of the nonpolar nature of ketone **1** it was imperative to decrease the overall charge of active center such that K163 and R415 were mutated into neutral residues. To further reduce the charge, we introduced another mutation at B:R88H, which is located along the subunit interface and close to the active center vicinity (Figure 4). Position 57 was mutated into phenylalanine, such that the phenyl ring of W57F simultaneously interacts with both ketone **1** and the side chain of I259M via a strong T-shaped π-stacking and a S/π interaction, respectively (Figure 4). In contrast, this interaction was not observed in W57G (Figure S5 in the Supporting Information). As a result of these mutations, in the best variant, the substrate's acetophenone core establishes T-shaped π-stacking interactions with the side chains of both B:F86 and F19, while the latter, in turn, interacts with B:F85 through a T-shaped π-stacking. The side chains of V422A and R415A also interact directly with ketone **1** via hydrophobic interactions. This extremely well-packed network of strong π-stacking interactions contributes greatly to a stable arrangement of ketone **1** in the active center pocket. The pose of ketone **1** is also catalytically preferable with the distance between the substrate carbonyl carbon and the PMP amino group being ~3.1 Å, which is very similar to the distance of 2.65 Å that has been reported for the PMP:acetophenone intermediate.[25]

In the first-round screening, position 153 nested at the subunit interface was mutated to the charged residues arginine and lysine, as well as to serine and alanine (Table S1). Although the most commonly observed amino acids at this position are arginine and glutamate, according to the homologous sequences studied (Figure S4), the results of the screening and further structural analysis clearly indicated that adding a charged residue at this position was not beneficial to the activity. Therefore, we propose that the introduction of negative charge would negatively affect the overall hydrophobicity of the active center, which is not ideal for our substrate. Thus, in the second round of screening, only mutant

DOI: 10.1021/acscatal.6b02380
ACS Catal. 2016, 6, 7749−7759

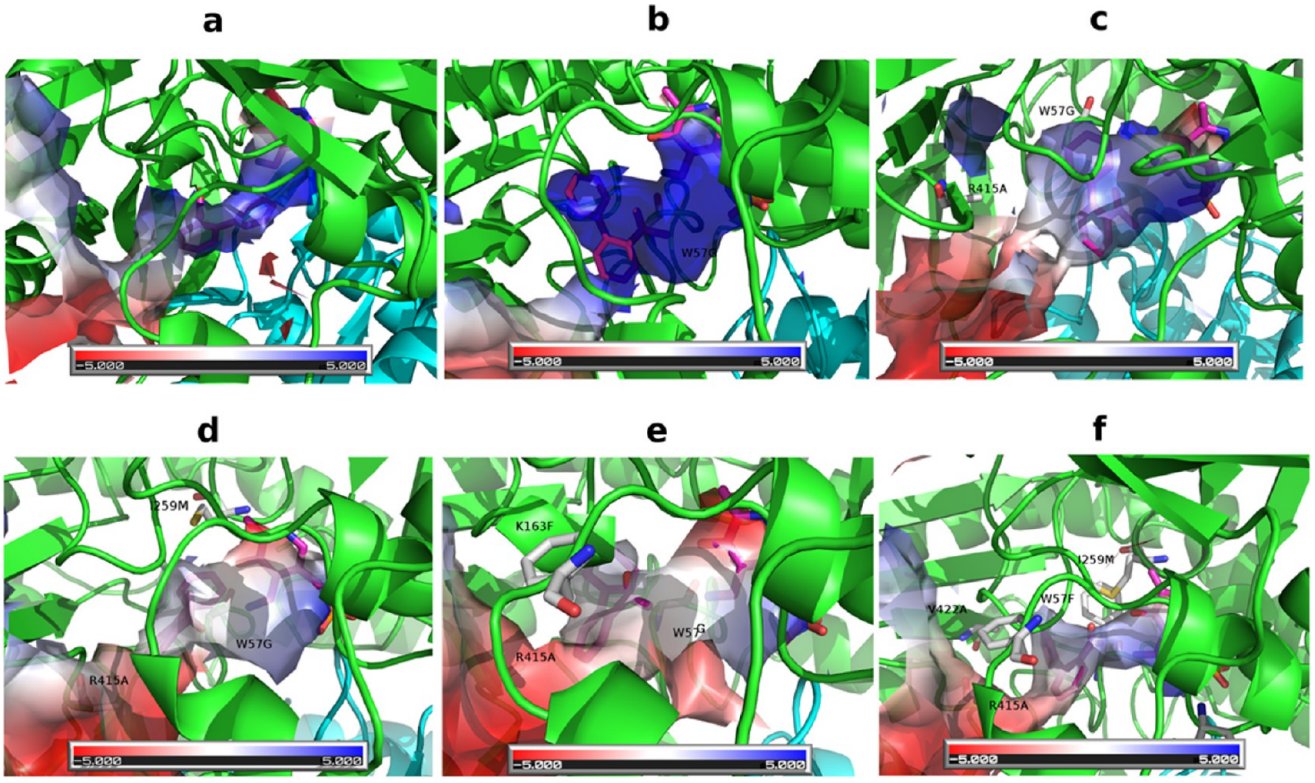

Figure 5. Electrostatic potential (±5 kT/e) of the MD reference structures of the *V. fluvialis* TAm (ketone **1** was docked in the presence of PMP) plotted on the solvent-accessible surface of the detected cavities: (a) WT TAm, (b) TAm_W57G, (c) TAm_W57G/R415A, (d) TAm_W57G/I259M/R415A, (e) TAm_W57G/K163F/R415A, and (f) TAm_W57F/R88H/V153S/K163F/I259M/R415A/V422A. Graphs (a)−(e) indicate a progression of colors from blue (positive) to red (negative).

V153S was considered. Mutating the valine residue 153 into serine can introduce additional interactions with Chain B via an ion-dipole interaction with K126 and a dipole−dipole interaction with H319 (see Figure S6 in the Supporting Information). We calculated changes in binding free energy ($\Delta\Delta G$) in the variant TAm_V153S using ZEMu.[21] The $\Delta\Delta G_{V153S}$ value obtained was −2.01 kcal/mol, which indicates that V153S mutation may increase the subunit interface affinity, and, hence, the overall structural stability of the enzyme (Figure S6).

Stability of the WT and engineered enzymes was examined *in vitro*. After 18 h, the best variant retains 98% and 90% of activity at 40 and 50 °C, respectively, while the other variants suffer a significant decrease in activity at 50 °C (see Tables S3 and S4 in the Supporting Information).

Active Center Polarity. The active center of the WT enzyme is positively charged (Figure 5a). Changing the polarity of the active site pocket was essential to better accommodate our nonpolar substrate to increase its conversion (Figure 5). In the mutant *V. fluvialis* TAm W57G/R415A, the charge of the active center becomes less positive and more delocalized (Figure 5c). Substitution of the bulky hydrophobic W57 with glycine enlarges the active site pocket (Figure 5b) and the simultaneous substitution of the positively charged R415 with an alanine reduces its positive charge (Figure 5c). In the subsequent engineering of the enzyme, this double mutant is conjugated with the K163F mutation that further contributes to decrease in the positive charge of the active center (Figure 5e). In the best variant, *V. fluvialis* TAm W57F/R88H/V153S/K163F/I259M/R415A/V422A, the positive charges of residues R88, K163, and R415 are completely removed. Simultaneously, the W57F, I259M, and V422A mutations introduce a well-packed hydrophobic network, making the binding pocket more compact and the active center substantially more neutrally charged (Figure 5f).

The combined effect of the favorable interactions and changes in active site polarity provides a valid explanation for the experimentally observed activity of the best variant (Table 1).

Selectivity. In the second half-reaction of the generally accepted mechanism for *ω*-TAm (Figure 1), the amino acceptor and the PMP co-factor react, leading to the formation of a ketimine intermediate. This is followed by proton abstraction and consequent electronic rearrangement of the ketimine intermediate, which is subsequently converted into a planar quinonoid intermediate. In the next step, the side chain of the catalytic lysine donates a proton to the nitrogen binding carbon of the planar quinonoid and an external aldimine intermediate is formed. It is at this point that the reaction specificity is determined. The half-reaction ends with the release of the product amine and the formation of a Schiff base (internal aldimine) between the aldehyde group of PLP and the side chain of the catalytic lysine. Thus, in order to assess the enantioselectivity of the mutants, we focused on the study of the planar quinonoid and the pro-(S) external aldimine intermediates (Figures S7b and S7c in the Supporting Information). The spatial arrangement of the catalytic lysine, with respect to the planar quinonoid, commands the orientation of the amino group of the catalytic lysine, which undergoes nucleophilic attack toward the nitrogen binding carbon of the quinonoid intermediate. This consequently dictates the chirality of the resulting external aldimine. We

DOI: 10.1021/acscatal.6b02380
ACS Catal. 2016, 6, 7749−7759

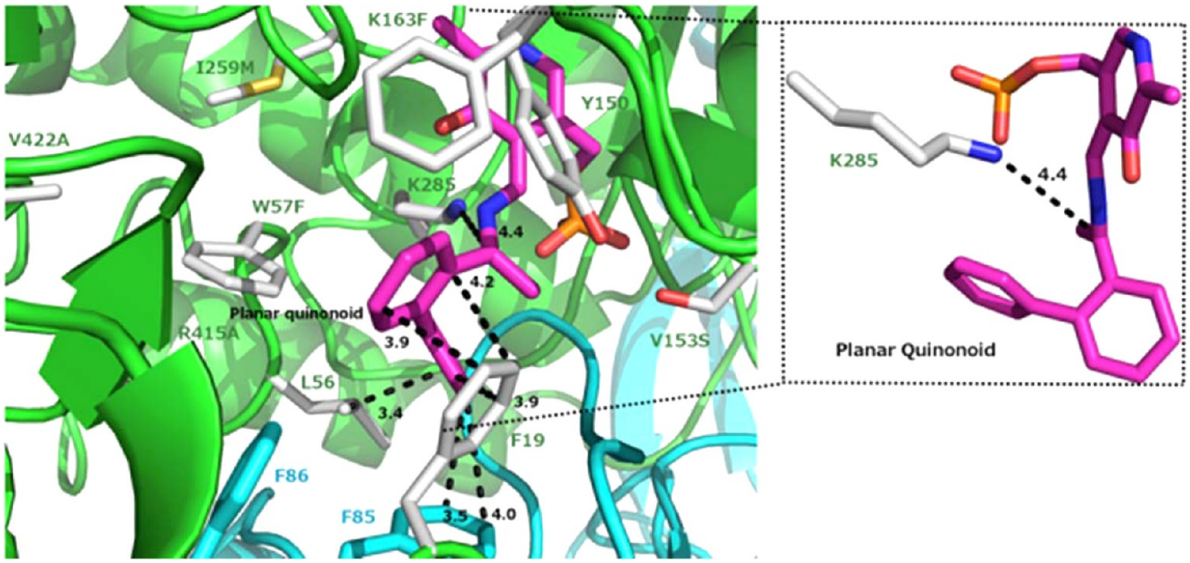

Figure 6. MD reference structure of *V. fluvialis* TAm W57F/R88H/V153S/K163F/I259M/V422A/R415A docked into the planar quinonoid. The active center residues are represented by sticks with the carbons of Chain A (green ribbon) colored in gray and the carbons of Chain B (cyan ribbon) colored in cyan. Relevant distances are shown (in units of Å). The MD reference structure corresponds to the structure with lowest RMSD (α-C atoms), relative to the average structure of the simulation. No significant changes were observed in the MD replicas.

observed that the spatial arrangement of all the variants favors the formation of pro-(S) external aldimine and, consequently, the formation of the end S-amine product (see Figure 6, as well as Figures S8 and S9 in the Supporting Information). For the *best* variant, TAm_W57F/R88H/V153S/K163F/I259M/R415A/V422A, we also conducted a MD analysis of the pro-(S) external aldimine. Superimposing of the MD reference structures of the planar quinonoid intermediate and the pro-(S) external aldimine demonstrates that the intermediates share an identical active center pose, which further indicates the (S)-chiral amine is the end product synthesized by the designed variant (see Figure S10 in the Supporting Information).

In the subsequent *in vitro* analysis, it was confirmed that all the described mutants produce the S-amine with an enantiomeric excess (ee) of >99% (Table 1).

CONCLUSIONS

We rationally engineered the (S)-selective TAm from *V. fluvialis* to catalyze conversion of the bulky 2-acetylbiphenyl to the corresponding (S)-amine. To improve substrate binding and conversion, we focused on enlarging the large binding pocket while increasing hydrophobicity at positions of W57, M259, V422, and R415, decreasing the charge of the active center at positions K163, R415, and B:R88 and improving the enzyme structural stability at position V153. With a minimal number of seven mutations, we designed an enzyme that shows an outstanding improvement in reaction rate (more than 1716-fold) and yields an enantiomeric pure (S)-amine product with an ee value of >99%. This variant retains 90% of the activity for 18 h at 50 °C.

It is noteworthy that the WT enzyme does not show any detectable activity toward 2-acetylbiphenyl. Our data showed that initial weak promiscuous activities toward a substrate are not always a necessity for enzyme evolution. By correctly selecting functionally relevant mutations, multistep rational mutagenesis can successfully provide a more efficient pathway for evolution, while nature most commonly follows smooth weak trade-off routes, hence requiring a substantial number of sequence modifications to gain a new function (i.e., new mutations accumulate while maintaining the robust native activity). Our results show that TAm displays a high plasticity, enabling us to evolve it with few mutations, starting from an enzyme with no detectable initial promiscuous activity toward a bulky ketone substrate such as 2-acetylbiphenyl.

ASSOCIATED CONTENT

Supporting Information

The Supporting Information is available free of charge on the ACS Publications website at DOI: 10.1021/acscatal.6b02380.

Additional figures and tables (PDF)

AUTHOR INFORMATION

Corresponding Author

*E-mail: m.huang@qub.ac.uk.

Author Contributions

[∇]These authors contributed equally.

Notes

The authors declare no competing financial interest.

ACKNOWLEDGMENTS

The authors acknowledge the financial support from INVEST NI Research and Development Programme, part financed by the European Regional Development Fund under the Investment for Growth and Jobs programme 2014-2020. We are grateful for the computing resources from QUB high performance computing Centre.

REFERENCES

(1) Nguyen, L. A.; He, H.; Pham-Huy, C. *Int. J. Biomed Sci.* **2006**, *2*, 85−100.

(2) (a) Taylor, P. P.; Pantaleone, D. P.; Senkpeil, R. F.; Fotheringham, I. G. *Trends Biotechnol.* **1998**, *16*, 412−418. (b) Koszelewski, D.; Tauber, K.; Faber, K.; Kroutil, W. *Trends Biotechnol.* **2010**, *28*, 324−332. (c) Höhne, M.; Bornscheuer, U. T. *ChemCatChem* **2009**, *1*, 42−51.

DOI: 10.1021/acscatal.6b02380
ACS Catal. 2016, 6, 7749−7759

(3) Silverman, R. B. *Organic Chemistry of Enzyme-Catalyzed Reactions*. 2nd Edition; Academic Press: San Diego, CA, 2002; p 800.
(4) (a) Shin, J. S.; Kim, B. G. *J. Org. Chem.* **2002**, *67*, 2848−53. (b) Steffen-Munsberg, F.; Vickers, C.; Thontowi, A.; Schatzle, S.; Meinhardt, T.; Svedendahl Humble, M.; Land, H.; Berglund, P.; Bornscheuer, U. T.; Hohne, M. *ChemCatChem* **2013**, *5*, 154−157.
(5) Savile, C. K.; Janey, J. M.; Mundorff, E. C.; Moore, J. C.; Tam, S.; Jarvis, W. R.; Colbeck, J. C.; Krebber, A.; Fleitz, F. J.; Brands, J.; Devine, P. N.; Huisman, G. W.; Hughes, G. J. *Science* **2010**, *329*, 305−309.
(6) (a) Midelfort, K. S.; Kumar, R.; Han, S.; Karmilowicz, M. J.; McConnell, K.; Gehlhaar, D. K.; Mistry, A.; Chang, J. S.; Anderson, M.; Villalobos, A.; Minshull, J.; Govindarajan, S.; Wong, J. W. *Protein Eng., Des. Sel.* **2013**, *26*, 25−33. (b) Park, E. S.; Park, S. R.; Han, S. W.; Dong, J. Y.; Shin, J. S. *Adv. Synth. Catal.* **2014**, *356*, 212−220. (c) Han, S. W.; Park, E. S.; Dong, J. Y.; Shin, J. S. *Adv. Synth. Catal.* **2015**, *357*, 2712−2720. (d) Han, S. W.; Park, E. S.; Dong, J. Y.; Shin, J. S. *Adv. Synth. Catal.* **2015**, *357*, 1732−1740. (e) Nobili, A.; Steffen-Munsberg, F.; Kohls, H.; Trentin, I.; Schulzke, C.; Hohne, M.; Bornscheuer, U. T. *ChemCatChem* **2015**, *7*, 757−760. (f) Genz, M.; Vickers, C.; van den Bergh, T.; Joosten, H. J.; Dorr, M.; Hohne, M.; Bornscheuer, U. T. *Int. J. Mol. Sci.* **2015**, *16*, 26953−63. (g) Cho, B. K.; Park, H. Y.; Seo, J. H.; Kim, J.; Kang, T. J.; Lee, B. S.; Kim, B. G. *Biotechnol. Bioeng.* **2008**, *99*, 275−84. (h) Pavlidis, I. V.; Weiß, M. S.; Genz, M.; Spurr, P.; Hanlon, S. P.; Wirz, B.; Iding, H.; Bornscheuer, U. T. *Nat. Chem.* **2016**, DOI: 10.1038/nchem.2578.
(7) Frisch, M. J.; Trucks, G. W.; Schlegel, H. B.; Scuseria, G. E.; Robb, M. A.; Cheeseman, J. R.; Scalmani, G.; Barone, V.; Mennucci, B.; Petersson, G. A.; Nakatsuji, H.; Caricato, M.; Li, X.; Hratchian, H. P.; Izmaylov, A. F.; Bloino, J.; Zheng, G.; Sonnenberg, J. L.; Hada, M.; Ehara, M.; Toyota, K.; Fukuda, R.; Hasegawa, J.; Ishida, M.; Nakajima, T.; Honda, Y.; Kitao, O.; Nakai, H.; Vreven, T.; Montgomery, J. A., Jr.; Peralta, J. E.; Ogliaro, F.; Bearpark, M.; Heyd, J. J.; Brothers, E.; Kudin, K. N.; Staroverov, V. N.; Kobayashi, R.; Normand, J.; Raghavachari, K.; Rendell, A.; Burant, J. C.; Iyengar, S. S.; Tomasi, J.; Cossi, M.; Rega, N.; Millam, J. M.; Klene, M.; Knox, J. E.; Cross, J. B.; Bakken, V.; Adamo, C.; Jaramillo, J.; Gomperts, R.; Stratmann, R. E.; Yazyev, O.; Austin, A. J.; Cammi, R.; Pomelli, C.; Ochterski, J. W.; Martin, R. L.; Morokuma, K.; Zakrzewski, V. G.; Voth, G. A.; Salvador, P.; Dannenberg, J. J.; Dapprich, S.; Daniels, A. D.; Farkas, Ö.; Foresman, J. B.; Ortiz, J. V.; Cioslowski, J.; Fox, D. J. *Gaussian 09, Revision A*; Gaussian, Inc.: Wallingford, CT, 2009.
(8) (a) Lee, C. T.; Yang, W. T.; Parr, R. G. *Phys. Rev. B: Condens. Matter Mater. Phys.* **1988**, *37*, 785−789. (b) Becke, A. D. *J. Chem. Phys.* **1993**, *98*, 5648−5652.
(9) Carvalho, A. T. P.; Teixeira, A. F. S.; Ramos, M. J. *J. Comput. Chem.* **2013**, *34*, 1540−1548.
(10) Miertus, S.; Scrocco, E.; Tomasi, J. *Chem. Phys.* **1981**, *55*, 117−129.
(11) Bayly, C. I.; Cieplak, P.; Cornell, W. D.; Kollman, P. A. *J. Phys. Chem.* **1993**, *97*, 10269−10280.
(12) Guex, N.; Peitsch, M. C. *Electrophoresis* **1997**, *18*, 2714−23.
(13) (a) Morris, G. M.; Goodsell, D. S.; Halliday, R. S.; Huey, R.; Hart, W. E.; Belew, R. K.; Olson, A. J. *J. Comput. Chem.* **1998**, *19*, 1639−1662. (b) Huey, R.; Morris, G. M.; Olson, A. J.; Goodsell, D. S. *J. Comput. Chem.* **2007**, *28*, 1145−1152.
(14) Case, D. A.; Berryman, J. T.; Betz, R. M.; Cerutti, D. S.; Cheatham, T. E., III; Darden, T. A.; Duke, R. E.; Giese, T. J.; Gohlke, H.; Goetz, A. W.; Homeyer, N.; Izadi, S.; Janowski, P.; Kaus, J.; Kovalenko, A.; Lee, T. S.; LeGrand, S.; Li, P.; Luchko, T.; Luo, R.; Madej, B.; Merz, K. M.; Monard, G.; Needham, P.; Nguyen, H.; Nguyen, H. T.; Omelyan, I.; Onufriev, A.; Roe, D. R.; Roitberg, A.; Salomon-Ferrer, R.; Simmerling, C. L.; Smith, W.; Swails, J.; Walker, R. C.; Wang, J.; Wolf, R. M.; Wu, X.; York, D. M.; Kollman, P. A. *Amber 2015*; University of California: San Francisco, CA, 2015.
(15) Hornak, V.; Abel, R.; Okur, A.; Strockbine, B.; Roitberg, A.; Simmerling, C. *Proteins: Struct., Funct., Genet.* **2006**, *65*, 712−725.
(16) Wang, J. M.; Wolf, R. M.; Caldwell, J. W.; Kollman, P. A.; Case, D. A. *J. Comput. Chem.* **2005**, *26*, 114−114.
(17) Ryckaert, J. P.; Ciccotti, G.; Berendsen, H. J. C. *J. Comput. Phys.* **1977**, *23*, 327−341.
(18) Darden, T.; York, D.; Pedersen, L. *J. Chem. Phys.* **1993**, *98*, 10089−10092.
(19) Kuipers, R. K.; Joosten, H. J.; Verwiel, E.; Paans, S.; Akerboom, J.; van der Oost, J.; Leferink, N. G. H.; van Berkel, W. J. H.; Vriend, G.; Schaap, P. J. *Proteins: Struct., Funct., Genet.* **2009**, *76*, 608−616.
(20) Kuipers, R. K.; Joosten, H. J.; van Berkel, W. J.; Leferink, N. G.; Rooijen, E.; Ittmann, E.; van Zimmeren, F.; Jochens, H.; Bornscheuer, U.; Vriend, G.; Martins dos Santos, V. A. P.; Schaap, P. J. *Proteins: Struct., Funct., Genet.* **2010**, *78*, 2101−13.
(21) Dourado, D. F. A. R.; Flores, S. C. *Proteins: Struct., Funct., Genet.* **2014**, *82*, 2681−2690.
(22) Flores, S.; Sherman, M.; Bruns, C.; Eastman, P.; Altman, R. *IEEE/ACM Trans. Comput. Biol. Bioinf.* **2011**, *8*, 1247−1257.
(23) Guerois, R.; Nielsen, J. E.; Serrano, L. *J. Mol. Biol.* **2002**, *320*, 369−87.
(24) Park, E. S.; Shin, J. S. *Enzyme Microb. Technol.* **2011**, *49*, 380−7.
(25) Cassimjee, K. E.; Manta, B.; Himo, F. *Org. Biomol. Chem.* **2015**, *13*, 8453−64.
(26) (a) Valley, C. C.; Cembran, A.; Perlmutter, J. D.; Lewis, A. K.; Labello, N. P.; Gao, J.; Sachs, J. N. *J. Biol. Chem.* **2012**, *287*, 34979−34991. (b) Ringer, A. L.; Senenko, A.; Sherrill, C. D. *Protein Sci.* **2007**, *16*, 2216−2223.
(27) Aledo, J. C.; Canton, F. R.; Veredas, F. J. *Sci. Rep.* **2015**, *5*, 16955.

DOI: 10.1021/acscatal.6b02380
ACS Catal. 2016, 6, 7749−7759